NUMERICAL SIMULATION OF ELONGATION AND MERGING OF BAY MOUTH SAND SPITS USING THE BG MODEL

Shusuke Watanabe[1], Takaaki Uda[2], Masumi Serizawa[1] and Shiho Miyahara[1]

The elongation and merging of bay mouth sand spits due to waves were numerically simulated using the BG model (a three-dimensional model for predicting beach changes based on Bagnold's concept). A bay separated by sandy headlands on both sides was assumed, and the topographic changes were predicted by the model. The wave-sheltering effect of the sand spit located offshore of the other sand spit played an important role in the mergence of the sand spits. The predicted results for the formation of sand spits were in good agreement with those given by Zenkovich (1967).

Keywords: Bay mouth; sand spit; BG model; prediction of beach changes

INTRODUCTION

A bay is a body of water separated by headlands on both sides. Zenkovich (1967) showed an aerial photograph (Fig. 1) of a fjord in eastern Kamchatka, as an example of a barrier beach extended at the bay mouth together with several examples of sand spits formed at the bay mouth. The elongation of such sand spits is commonly observed not only at bay mouths but also at river mouths, where the direction of the shoreline abruptly changes, and in some cases it causes the deposition of sand in navigation channels in the vicinity of sand spits or the closure of a river mouth. Thus, the study of the development of sand spits and the prediction of successive changes in sand spits are important in coastal engineering. Consider a case in which the coasts on both sides of a bay are composed of unconsolidated layers. In this case, sea cliffs are formed and sand supplied from the cliffs can be deposited to form sand spits near the bay mouth. When the water depth of the sand deposition zone is small, the sand bars can extend to form a bay barrier enclosing the bay. Uda and Serizawa (2011) investigated the formation of a bay barrier for different depths of a body of water using the BG model (a three-dimensional model for predicting beach changes based on Bagnold's concept), and concluded that a sand bar rapidly extends to form a bay barrier when the water depth is small, whereas a bay barrier cannot be formed in case of a larger water depth. They predicted the extension of symmetrical sand bars from both sides in the case of a flat seabed. The shape of the bay, however, is not always symmetrical. When sand spits develop from both shores, the sand spit located offshore has a wave-sheltering effect on the other spit, affecting the topographic changes of the other sand spit, and finally the two spits merge. In this study, the elongation and merging of sand spits at a bay mouth were investigated using the BG model.

FORMATION OF BAY BARRIERS

Figure 1, taken from Zenkovich (1967), is an example of a barrier beach formed by the deposition of gravel in a bay. Although the scale and direction are not given in Fig. 1, waves can be assumed to be incident from the upper part owing to the configuration of the bay mouth bar. This wave incidence caused longshore sand transport along the shorelines on both sides of the bay, and sand was deposited to form the sand spits that developed from both shores. Then, the sand spits connected each other, resulting in the formation of a barrier beach. Note that the beach is wide at the central part of the bay barrier, whereas it is narrow at the right end.

Zenkovich (1967) showed another example of a sand spit formed in a bay mouth (Fig. 2). A shows an example of sand spits alternately extending from both shores of the bay mouth and B shows another example in which a slender sand spit extended owing to unidirectional longshore sand transport from the right bank. Figure 3 shows another example of a pair of sand spits. The tips of the sand spits extended on both sides of the bay markedly curved inward. This is because the water depth at the tips of the sand spits is too larger for the sand spits to extend in a straight line, as shown by Uda and Serizawa (2011). Here, the development of bay barriers, as mentioned above, was investigated using the BG model.

[1] Coastal Engineering Laboratory Co., Ltd., 1-22-301 Wakaba, Shinjuku, Tokyo 160-0011, Japan
[2] Public Works Research Center, 1-6-4 Taito, Taito, Tokyo 110-0016, Japan

Figure 1. Bay barrier closing bay mouth in fjord in eastern Kamchatka (Zenkovich, 1967).

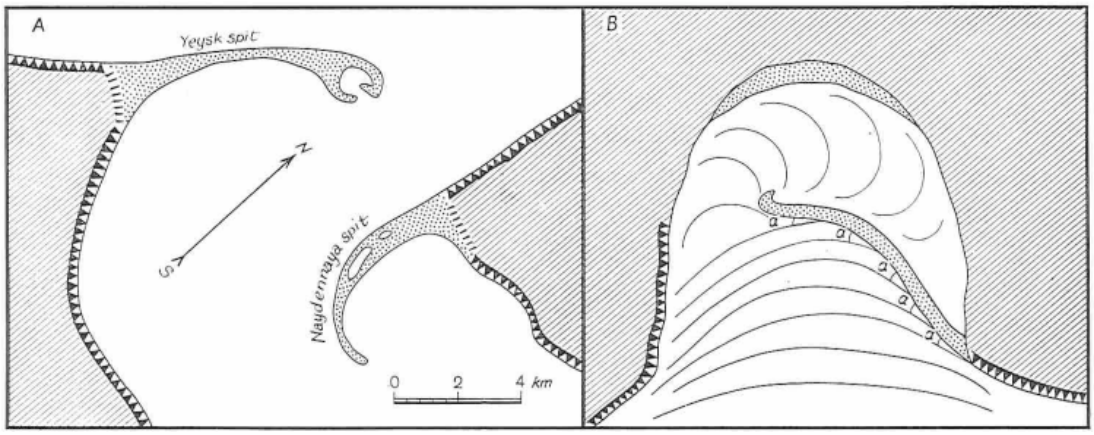

Zenkovich (1967, p.438, Fig. 214)

Figure 2. Schematic diagram of formation of bay mouth sand spits (Zenkovich, 1967).

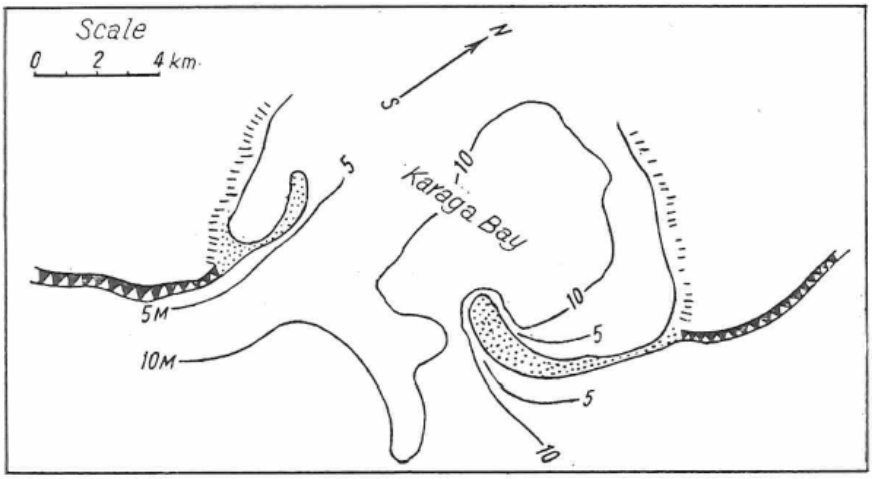

Figure 3. Example of a pair of sand spits enclosing Karaga Bay (Zenkovich, 1967).

THE BG MODEL FOR PREDICTING BEACH CHANGES

The sand transport equation employed in this study is Eq. (1), which uses an expression for the wave energy evaluated at the breaking point, also employed in Serizawa et al. (2006) and Uda et al. (2012). The variables in Eq. (1) are given by Eqs. (2) - (10).

$$\vec{q} = C_0 \frac{K_s P}{\tan\beta_c}\left\{\tan\beta_c \vec{e_w} - |\cos\alpha|\ \overrightarrow{\nabla Z}\right\} \qquad \left(-h_c \le Z \le h_R\right) \tag{1}$$

$$P = \varepsilon(Z)\left(EC_g\right)_b \tan\beta_w \qquad \left(\mathrm{P} \ge 0\right) \tag{2}$$

$$\tan\beta_w = dZ / dx_w \qquad \left(\tan\beta_w \ge 0\right) \tag{3}$$

$$\int_{-h_c}^{h_R} \varepsilon(Z) dZ = 1 \tag{4}$$

$$\varepsilon(Z) = \begin{cases} \dfrac{1}{h_c + h_R} & \left(-h_c \le Z \le h_R\right) \\ 0 & \left(Z < -h_c,\ Z > h_R\right) \end{cases} \tag{5}$$

$$I_\varepsilon(Z) = \begin{cases} 1 & \left(Z < -h_c\right) \\ \displaystyle\int_Z^{h_R} \varepsilon(Z)\, dZ = \frac{h_R - Z}{h_c + h_R} & \left(-h_c \le Z \le h_R\right) \\ 0 & \left(Z > h_R\right) \end{cases} \tag{6}$$

$$P = \left(EC_g\right)_b \left(-\frac{dI_\varepsilon}{dx_w}\right) \qquad \left(P \ge 0\right) \tag{7}$$

$$I_\varepsilon^{(i+1)} = \min\left(Eq.\ (6)\Big|^{Z=Z^{(i+1)}},\ I_\varepsilon^{(i)}\right) \tag{8}$$

$$P^{(i+1/2)} = \left(EC_g\right)_b \left(\frac{I_\varepsilon^{(i)} - I_\varepsilon^{(i+1)}}{\Delta x_w}\right) \tag{9}$$

$$\left(EC_g\right)_b = C_1 \left(H_b\right)^{\frac{5}{2}} \approx C_1 \left(H_{1/3}\right)^{\frac{5}{2}} \tag{10a}$$

$$C_1 = \frac{\rho g}{k_1}\sqrt{g/\gamma} \qquad \left(\ k_1 = \left(4.004\right)^2,\ \gamma = 0.8\ \right) \tag{10b}$$

Here, $\vec{q} = \left(q_x,\ q_y\right)$ is the net sand transport flux, Z (x, y, t) is the seabed elevation with reference to the still water level (Z = 0), $\overrightarrow{\nabla Z} = \left(\partial Z/\partial x,\ \partial Z/\partial y\right)$ is the seabed slope vector, $\vec{e_w}$ is the unit vector in the wave direction, α is the angle between the wave direction and the direction normal to the contour line, x_w is the coordinate along the direction of wave propagation, tanβ_w is the seabed slope measured along the direction of wave propagation, tanβ_c is the equilibrium slope of sand and K_s is the longshore and cross-shore sand transport coefficient. C_0 is the coefficient transforming the immersed weight expression to a volumetric expression ($C_0 = 1/\left\{\left(\rho_s - \rho\right) g\left(1-p\right)\right\}$; ρ is the seawater density, ρ_s is the specific gravity of sand, p is the porosity of sand, and g is the acceleration due to gravity), h_c is the depth of closure, and h_R is the berm height.

$\varepsilon(Z)$ in Eq. (5) is the depth distribution of sand transport, $(EC_g)_b$ is the wave energy flux at the breaking point, H_b is the breaker height, $H_{1/3}$ is the significant wave height of the incident waves and γ

is the ratio of the breaker height to the water depth. As the beach slope in Eq. (2), the local beach slope measured along a wave ray was used. The index i in Eqs. (8) and (9) is the mesh number along the x_w-axis, and min means the selection of the smaller of either value in parentheses.

To calculate the P value in Eq. (7), another coordinate system different from that employed for the calculation of beach changes was used (Uda et al., 2012), in which the x_w- and y_w-axes were taken along the wave direction and normal direction, respectively, as shown in Fig. 4. A fixed coordinate system (x, y) is used for the calculation of beach changes with the rectangular calculation domain ABCD, whereas the P value was calculated in the rectangular domain A'B'C'D', which has the coordinate system (x_w, y_w) and includes the domain ABCD. In the wave calculation, wave refraction was neglected and waves were assumed to propagate in a straight manner, while maintaining their incident angle.

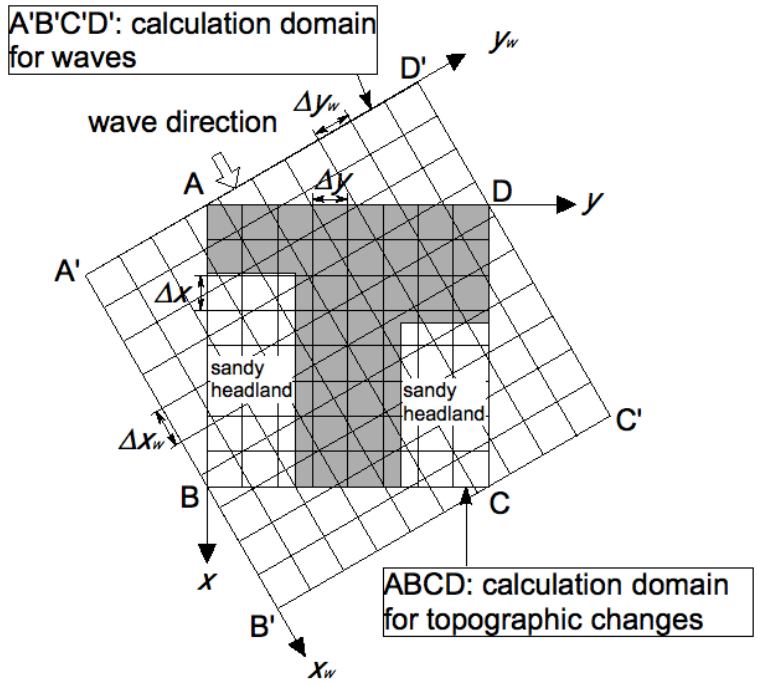

Figure 4. Arrangement of calculation domains.

The distance along the x_w-axis is subdivided by a mesh of size Δx_w, and a cumulative function of $\varepsilon(Z)$ is introduced as Eq. (6). Here, $\varepsilon(Z)$ is assumed to have a uniform distribution and $I_\varepsilon(Z)$ is a function that takes a value of unity in the zone deeper than the depth of closure, decreases with the water depth and becomes 0 in the zone higher than the berm height. Using Eq. (6), Eq. (2) is transformed into Eq. (7). Thus, the P value can be determined from the derivative of $I_\varepsilon(Z)$ at a point along the x_w-axis using Eq. (7). $I_\varepsilon(Z)$ is calculated along the x_w-axis from the starting point of wave incidence in the direction of wave propagation; $I_\varepsilon(Z)$ at the $(i+1)^{\text{th}}$ point can be calculated from Eq. (8) with the given value of $I_\varepsilon(Z)$ at the i^{th} point when the initial value of $I_\varepsilon(Z)$ at the offshore end is given and the mesh location is denoted by $x_w^{(i)} = i\Delta x_w$. Furthermore, the P value at the $(i+1/2)^{\text{th}}$ point is calculated from Eq. (9), which is the discretized form of Eq. (7). Note that in calculating $I_\varepsilon(Z)$ at the $(i+1)^{\text{th}}$ point, the smaller of the values calculated from Eq. (6) given the elevation $Z(i+1)$ at the $(i+1)^{\text{th}}$ point and $I_\varepsilon(Z)$ at the ith point is adopted. As a result, the value of $I_\varepsilon(Z)$ corresponding to the minimum water depth (maximum Z) between the offshore end to a designated point along the x_w-axis can be adopted, regardless of the functional form of $\varepsilon(Z)$ that is adopted.

Using this procedure, the depth distribution along the x_w-axis between the offshore end and a certain point is automatically taken into account in the calculation of the P value. For example, when there is a location with an elevation higher than the berm height, the P value in the shoreward zone is automatically reset to 0, regardless of the elevation and water depth. This procedure becomes important

when the beach profile along the x_w-axis has several uneven shapes.

Consider the case wherein the x_w-axis passes near the tips of two sand spits. The wave energy is reduced when waves pass near the tip of the first sand spit, resulting in the reduction of the wave energy reaching the second sand spit. Using this procedure, the wave-sheltering effect due to the existence of multiple sand spits can be automatically evaluated, in contrast to the method whereby the P value is calculated by substituting the local elevation Z into $\varepsilon(Z)$ in Eq. (2).

In addition, the P value integrated from a location on land where the elevation exceeds the berm height to an offshore point along the x_w-axis is always equivalent to the wave energy flux at the breaking point $(EC_g)_b$, regardless of the seabed topography. Because $(EC_g)_b$ corresponds to the total power of the incident waves, the exact satisfaction of this condition is reasonable.

The calculation of the P value was independently carried out along each x_w-axis. The P value calculated at the point (x_w, y_w) was memorized and the P value at the point (x, y) necessary for the calculation of beach changes was interpolated from the memorized value at the point (x_w, y_w). The mesh intervals of Δx_w and Δy_w are the same as those of Δx and Δy. The beach changes were calculated by explicitly solving the continuity equations ($\partial Z/\partial t + \nabla \bullet \vec{q} = 0$) on the staggered meshes using the sand transport fluxes obtained from Eq. (1). The P value, which changes with the propagation of waves, was recalculated at every calculation step of the beach changes. The wave direction at each step was randomly determined so that the probability of occurrence of each wave direction was satisfied. As the probability of occurrence, the directional distribution of wave energy that corresponds to the angular spreading parameter $S_{\max} = 10$ for wind waves was used by employing the angular spreading method for irregular waves (Uda, 2010). This is equivalent to the condition that multidirectional irregular waves with angular spreading were incident to the calculation domain.

In addition, when the ground elevation Z approaches the upper limit (h_R) or lower limit of beach changes ($-h_c$) during the calculation of beach changes, the sand transport rate was reduced by multiplying by a reduction ratio using the method of Uda et al. (2013), so that the beach changes do not occur outside these limits.

CALCULATION CONDITIONS

A rectangular calculation domain with 600 m length in the longshore and cross-shore directions was used, and a flat solid seabed with a constant depth of 3 m was considered in this domain. Also, sandy headlands with an initial beach slope of 1/10 and a berm height of 1 m were set in a part of this domain. Although the headlands separating a bay are commonly composed of hard rocks with high resistance to wave abrasion, in this study, the headlands themselves were assumed to be made of sand to permit sand transport along the shorelines and the deformation of the headlands. The beach changes were predicted under the condition that waves with a significant wave height of 1 m were incident from the direction normal to the longshore direction. The depth of closure and the equilibrium slope of sand were assumed to be $h_c = 3$ m and 1/10, respectively. The calculation domain was discretized by meshes of $\Delta x = \Delta y = 10$ m. The time interval was $\Delta t = 1$ hr, and the calculation was carried out for up to 8000 steps (8000 hr). For the boundary conditions, sand transport was set to be 0 along the external boundary of the calculation domain. Table 1 shows the calculation conditions.

Table 1. Calculation conditions.

Incident wave height H	1 m
Berm height h_R	1 m
Depth of closure h_c	3 m
Equilibrium slope $\tan\beta_c$	1/10
Coefficients of sand transport	Coefficient of longshore sand transport $K_s = 0.2$ Coefficient of cross-shore sand transport $K_n = K_s$
Mesh size	$\Delta x = \Delta y = 10$ m
Time interval	$\Delta t = 2$ hr
Duration of calculation	8, 000 hr (8, 000 step)
Boundary conditions	Shoreward and landward ends $q_x = 0$ Right and left boundaries $q_y = 0$

Figure 5 shows the cases considered in the calculation. In Case 1, a slender, rectangular sandy headland was placed at the left end of the calculation domain. In Case 2, another sandy headland with the same shape as that on the left side was placed on the right side to form a symmetric arrangement. In Case 3, the slender, rectangular sandy headland on the left side was extended by 50 m in the direction of wave propagation and that on the right side was shortened by 100 m to form an asymmetric arrangement.

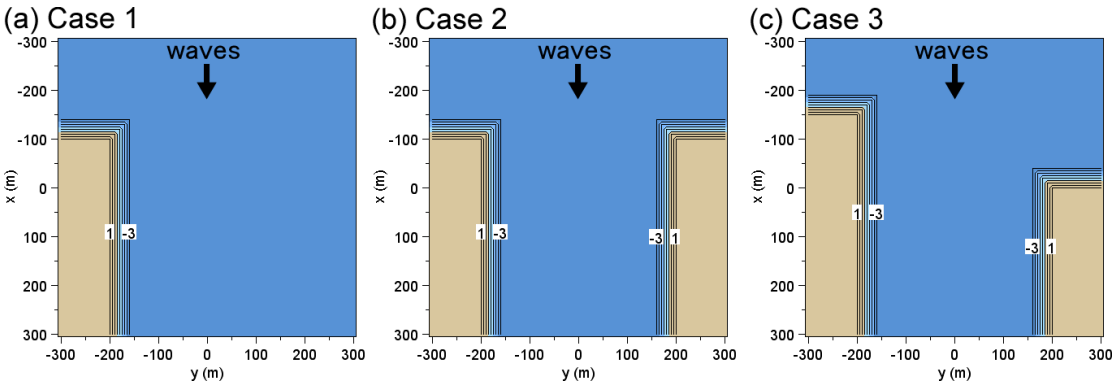

Figure 5. Cases considered in the calculation.

RESULTS OF CALCULATION

Single Sandy Headland (Case 1)

Figure 6 shows the results of the calculation up to 5000 hr in the case that a single, rectangular sandy headland was placed on the left side of the calculation domain. Under the initial condition, the sandy headland had a 440 m length and 240 m width in the x- and y-directions, respectively, and irregular waves with a significant wave height of 1 m were incident from the x-direction.

Initially, the shoreline direction changed by 90° at the corner between the exposed side of the rectangular sandy headland normal to the direction of wave propagation and its right side. When waves were incident from the x-direction, a spatial imbalance in longshore sand transport occurred near the corner, causing erosion to the left of the corner. Then, eroded sand was transported rightward, resulting in the formation of sand spit A at the corner (Fig. 6(b)). Simultaneously, shoreline undulation started to develop owing to the high-angle wave instability (Ashton and Murray, 2006) along the shoreline extending parallel to the direction of wave propagation because of the large incidence angle, and a small sand spit A' was formed. In the first 1000 hr, sand spit A extended by 60 m. After 2000 hr of wave action, sand spit A had further extended to a length of 120 m (Fig. 6(c)). Sand necessary for the formation of the sand spit was transported from the tip of the rectangular sandy headland at the initial stage, and the small sand spit A' further developed near the foot of the rectangular sandy headland. After 3000 hr, the sand spit A was significantly elongated, producing a wave-shelter zone in the lee of the sand spit (Fig. 6(d)). Sand spit A' located near the foot of the sandy headland disappeared owing to the wave-sheltering effect of sand spit A. With time, sand spit A further became elongated and had a length of 230 m after 4000 hr and a length of 280 m after 5000 hr (Figs. 6(e) and 6(f)).

As mentioned above, when irregular waves were incident from the x-direction to the rectangular sandy headland on the left side of the calculation domain, sand spits independently developed near the head and foot of the sandy headland at the initial stage. With increasing scale of the sand spit at the head, its wave-sheltering became dominant, and the sand spit formed at the foot of the sandy headland was included in its wave-shelter zone. Then, it disappeared, resulting in the rightward elongation of a single sand spit. This elongation of a single sand spit well explains the mechanism of the extension of sand spits given by Zenkovich (1967), as schematically shown in Fig. 2.

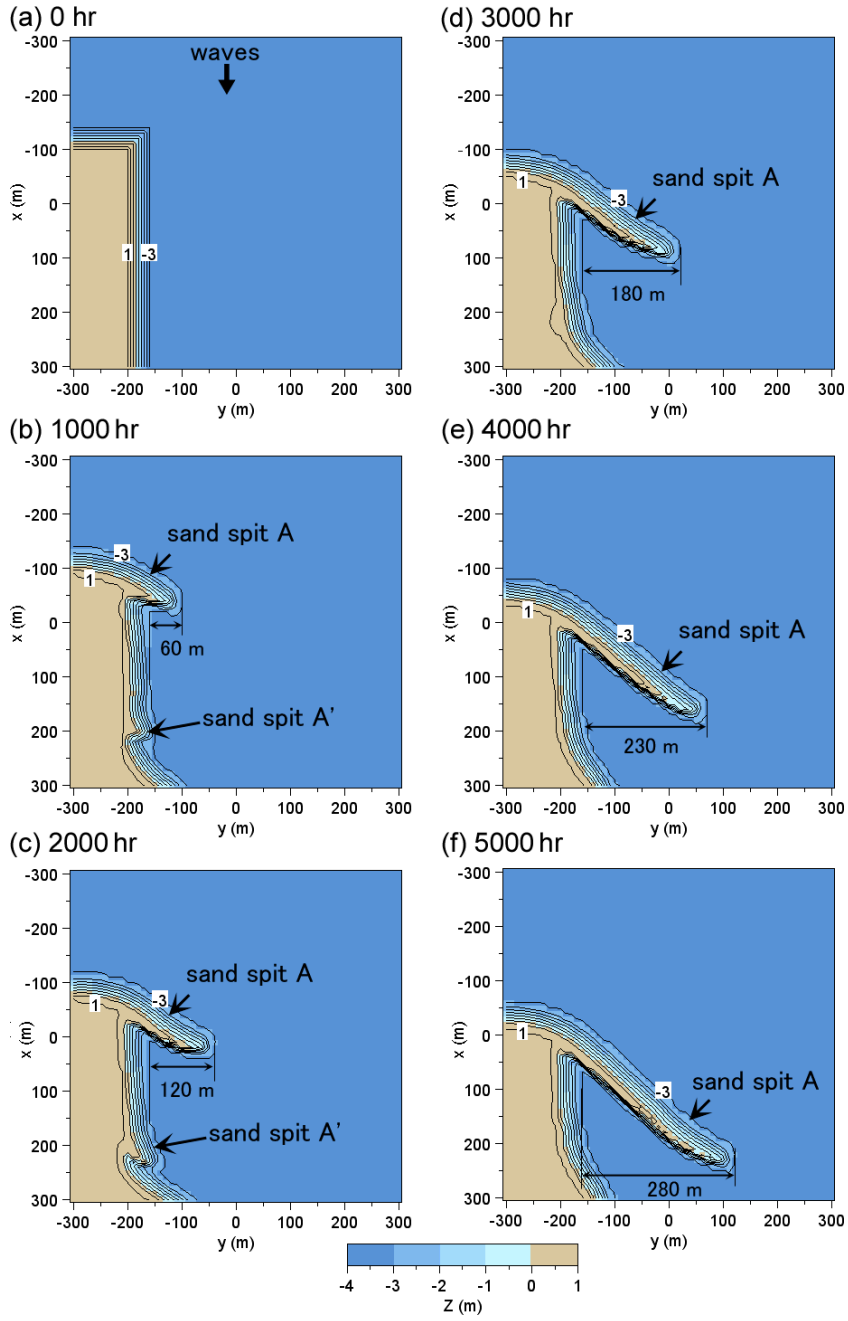

Figure 6. Calculation results for elongation of sand spit along the shoreline on right side of sandy headland (Case 1).

Deformation of Symmetric Sandy Headlands on Both Sides of a Bay (Case 2)

In Case 2, another slender, rectangular sandy headland with the same size as that in Case 1 existed on the right side of the bay to form a symmetrical arrangement. Figure 7 shows the calculation results up to 8000 hr. In Case 1, the shoreline on the right side of the single sandy headland was exposed to waves without any wave-sheltering effect from the other side of the bay. In contrast, in Case 2, sandy headlands were symmetrically arranged on both sides of the bay with a distance of 320 m between them. Therefore, the sandy headland on the left was subjected to the wave-sheltering effect from that on the right, and vice versa. When irregular waves were incident from the *x*-direction under these conditions, after 1000 hr three small-scale sand spits had developed along the shoreline on both sides of the sandy headlands, as shown in Fig. 7(b), together with the elongation of two slender sand spits, one on each side of the bay mouth, which had the same size as that in Case 1. Although a single sand spit developed along the shoreline on the side of the sandy headland in Case 1, three sand spits had formed

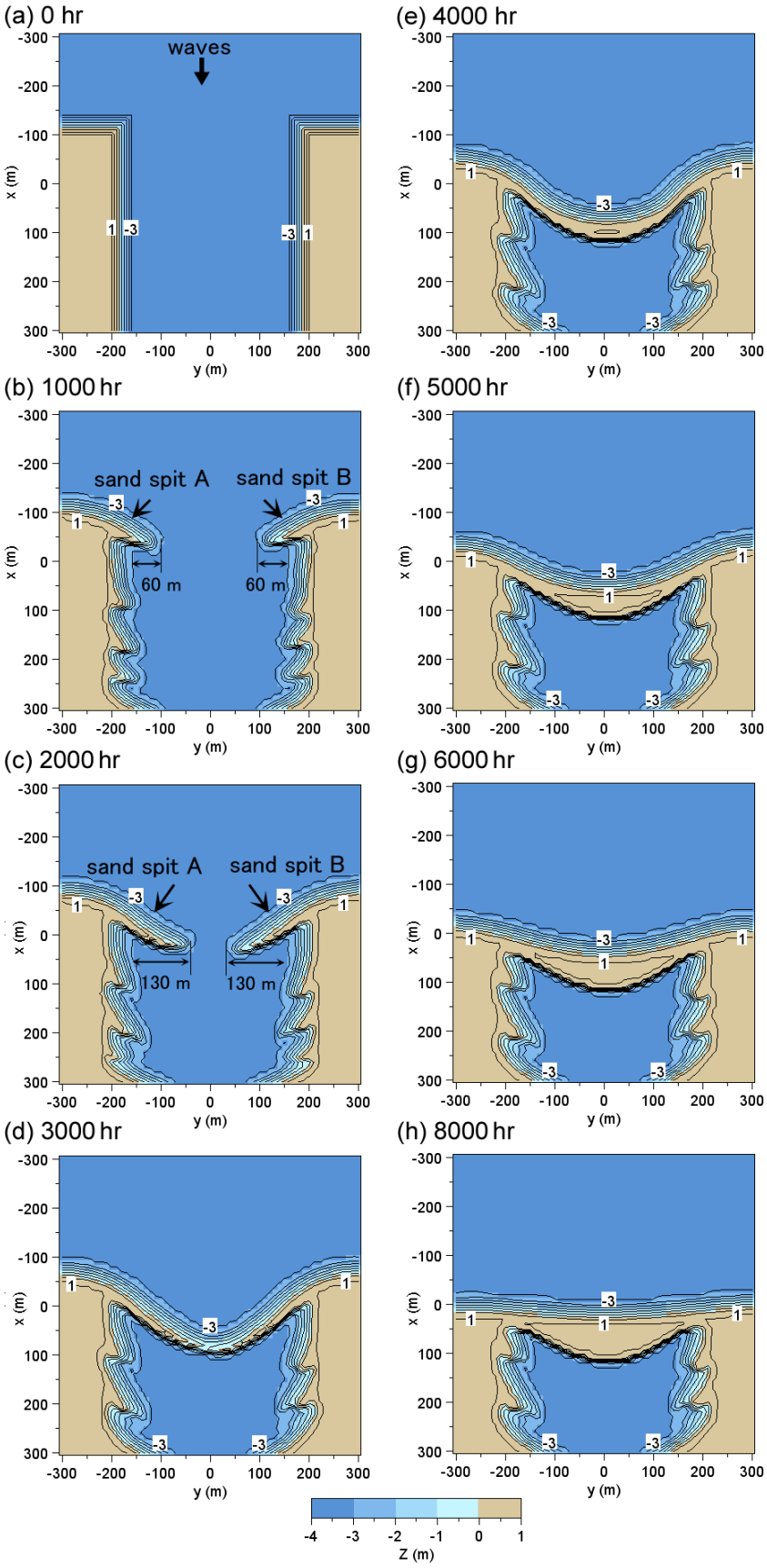

Figure 7. Calculation results for elongation of bay mouth bar between two sandy headlands separating a bay (Case 2: symmetric arrangement).

after 1000 hr in Case 2. After 2000 hr, the two slender sand spits at the bay mouth had further extended, and the opening width was narrowed to 60 m (Fig. 7(c)). On the other hand, because waves were obliquely incident to the sand spits on both sides of the sandy headlands through the opening between the bay mouth bars, these sand spits further developed. The scale of the three sand spits on both sides of the sandy headlands increased until 2000 hr. After 3000 hr, the two sand spits that extended from both sides had connected to form a bay barrier. Because the bay mouth was completely closed by the bay barrier, the sand spits that formed along the shoreline on both sides of the sandy headlands were left intact (Fig. 7(d)). Longshore sand transport from the sandy headlands to the concave shoreline still prevailed even after the complete closure of the bay mouth by the bay barrier, and the beach width at the central part of the bay barrier increased with time (Figs. 7(e), 7(f) and 7(g)). Beach changes continued until that the shoreline connecting the sandy headlands was straight (Fig. 7(h)).

In this study, two headlands were composed of sand on both sides of the bay to allow the movement of sand toward the inside of the bay. The shoreline on the sides of these sandy headlands was deformed owing to the high-angle wave instability mechanism, sand spits were rapidly formed and finally the shoreline connecting the sandy headlands became normal to the incident wave direction after 8000 hr. Comparing the shape of the bay barrier after 4000 hr, as shown in Fig. 7(e), with Fig. 1 from Zenkovich (1967), the calculation results illustrating the development of a bay barrier and a wide beach at the central part of the bay barrier are in good agreement with the photograph shown in Zenkovich (1967). Although the calculation conditions had some differences from that of the prototype topography in that both headlands enclosing the bay were rocky in Fig. 1, the existence of sand movement toward the bay bottom can be confirmed from Fig. 1 because of the formation of a hooked shoreline on the left side of the headland.

Deformation of Asymmetric Sandy Headlands on Both Sides of a Bay (Case 3)

In Case 3, the length of the sandy headlands on the left and right sides of the calculation domain in Case 2 was extended by 50 m and shortened by 100 m, respectively, in the x-direction to form an asymmetric arrangement of sandy headlands in the initial stage, as shown in Fig. 8(a). When waves were incident from the x-direction under this arrangement, the wave-sheltering effect of the left sandy headland on the right sandy headland became stronger because of the protrusion of the left sandy headland.

After 1000 hr, the sand spits had started to form on both sides of the sandy headlands (Fig. 8(b)). Here, the sand spits that started developing on the left and right sides of the bay are denoted as sand spits A and B, respectively, as shown in Fig. 8(b). At this stage, the elongation length of sand spits A and B was 60 m. Although undulations started to form along the shoreline on the sides of the sandy headlands as a result of the shoreline instability, the number of shoreline undulations was two on the right side of the bay and three on the left side, because the space where the shoreline undulations occurred was larger behind sand spit A.

With further wave action, sand spits A and B became markedly elongated to 120 and 130 m, respectively, after 2000 hr (Fig. 8(c)). Sand spit B was 10 m longer than sand spit A because of the larger wave-sheltering effect of sand spit A (Fig. 8 (c)). After 3000 hr, sand spit B had further elongated and the tip of the sand spit curved and approached the tip of sand spit A (Fig. 8(d)). After 4000 hr, sand spit B had stopped elongating because it had entered the wave-shelter zone of sand spit A, and the tip of sand spit A became connected to sand spit B owing to successive sand deposition near the tip of sand spit A (Fig. 8(e)). After 5000 hr, a bay barrier had formed by the connection of the two sand spits A and B extending from both sides. Although a symmetric bay barrier was formed in Case 2, as shown in Fig. 7, in Case 3, in which the slender sandy headlands were arranged asymmetrically, the width of the bay increased by the deposition of sand at the tip of sand spit B and a bay barrier with a wide shore in the central part was formed as shown in Fig. 8(f). With time, the bay barrier continued to develop up to 8000 hr, although a protrusion that had formed near the point connecting the two sand spits was left intact. This protrusion was formed when sand spit A was superimposed on sand spit B from the offshore side in the period between 4000 and 5000 hr, which corresponds to the previous beach changes in the evolution process of the bay barrier.

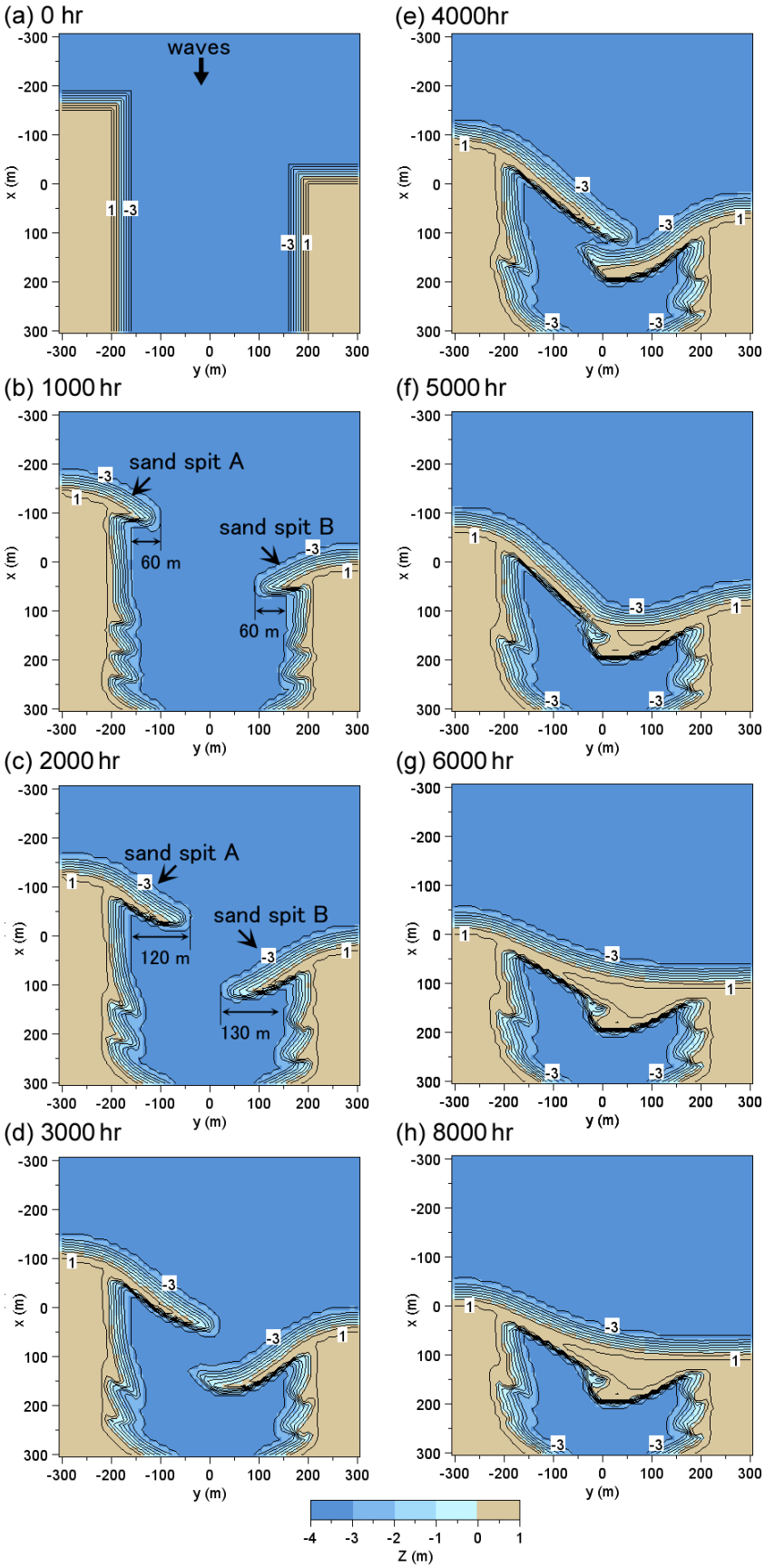

Figure 8. Calculation results for elongation of bay mouth bar between two sandy headlands separating a bay (Case 3: asymmetric arrangement).

CONCLUSIONS

The elongation and merging of sand spits formed at a bay mouth with symmetric and asymmetric shapes were investigated using the BG model. When a slender sandy headland was placed on the left side of the bay (Case 1), sand spits independently developed near the tip of the sandy headland and at the base of the sandy headland at the initial stage. With increasing scale of the sand spit formed near the tip of the sandy headland, the wave-sheltering effect increased and the sand spits that had formed near the base of the sandy headland were included in the wave-shelter zone and disappeared. Finally, a single sand spit extended to the right. The numerical results for the elongation of a single sand spit into a bay and an image in Zenkovich (1967) were in good agreement. In Case 2, in which another slender rectangular sandy headland with the same size as that in Case 1 was placed on the right side of the bay, the predicted formation of a bay barrier with a concave shape and a wide beach in the central part of the bay barrier was in good agreement with an image in Zenkovich (1967). Finally, when the sandy headlands were placed asymmetrically (Case 3), the wave-sheltering effect of the sand spit from the larger headland on the other sand spit was significant, and finally the sand spits merged with each other to form a single bay mouth barrier.

REFERENCES

Ashton, A. and Murray, A. B. 2006. High-angle wave instability and emergent shoreline shapes: 1. Modeling of sand waves, flying spits, and capes, *J. Geophys. Res*., Vol. 111, F04011, doi: 10.1029/2005JF000422.

Serizawa, M., Uda, T., San-nami, T. and Furuike, K. 2006. Three-dimensional model for predicting beach changes based on Bagnold's concept, *Proc. 30th ICCE*, pp. 3155-3167.

Uda, T. 2010. *Japan's Beach Erosion - Reality and Future Measures*, World Scientific, London, p. 418.

Uda, T. and Serizawa, M. 2011. Model for predicting formation of bay barriers in flat shallow sea, *Coastal Sediments '11*, pp. 1176-1189.

Uda, T., Serizawa, M. and Miyahara, S. 2012. Numerical simulation of three-dimensional segmentation of elongated water body using BG model, *Proc. 33rd ICCE*, pp. 1-11.

Uda, T., Gibo, M., Ishikawa, T., Miyahara, S., San-nami, T. and Serizawa, M. 2013. Change in carbonate beach triggered by construction of a bridge on Irabu Island and its simulation using BG model, *Asian and Pacific Coasts 2013, Proc. 7th International Conf*., pp. 24-31.

Zenkovich, V. P. 1967. *Processes of Coastal Development, Interscience Publishers*, New York, p. 751.